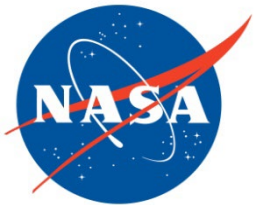

National Aeronautics and
Space Administration

HLS-PAP-039
REVISION A
RELEASE DATE: OCTOBER 12, 2023

HUMAN LANDING SYSTEM (HLS) PROGRAM NON-DESIGN DRIVER LUNAR ENVIRONMENTS

Publicly Available: Release to Public Websites Requires Approval of Chief, Office of Primary Responsibility, and approval via the Scientific and Technical Information (STI) process, if applicable

REVISION AND HISTORY PAGE

Revision No.	Change No.	Description	Release Date
-	n/a	Initial Baseline Release	03/13/2023
A	n/a	The technical information in the paper did not change from Baseline to Rev A. Rev A only affects changes to figures.	10/12/2023

TABLE OF CONTENTS

SECTION **PAGE**

APPENDIX

TABLE

FIGURE

1.0 INTRODUCTION

The space and lunar environments important for human-class spacecraft hardware design are defined in SLS-SPEC-159 Cross-Program Design Specification for Natural Environments (DSNE). This white paper documents additional lunar environments about which questions are frequently raised, but which do not impact hardware design. It will be revised as needed.

1.1 PURPOSE

The purpose of this white paper is to provide a source of information on lunar environments which, according to scientific and engineering consensus, should not impact human-class spacecraft design. Additionally, comparisons are shown between the Apollo missions and Artemis mission parameters for solar lighting angles at the landing sites and plasma region exposure.

1.2 SCOPE

This is an informational white paper intended to provide information on lunar environments which are not significant for human-class spacecraft design or operations. SLS-SPEC-159 DSNE documents environments required to be considered for spacecraft design and against which verifications must be completed. However, hardware designers may want to consider the magnitude of the environmental parameters described here in case there are particular sensitivities to them.

1.3 CHANGE AUTHORITY/RESPONSIBILITY

This is a data-managed rather than configuration-managed document. Proposed changes to this document should be submitted to the Human Landing System Natural Environments Discipline for consideration.

All such requests will adhere to the Human Landing System Configuration and Data Management Plan, documented in HLS-PLAN-004.

The appropriate NASA Office of Primary Responsibility (OPR) identified for this document is the Human Landing System Natural Environments Discipline which reports to HLS Systems Engineering and Integration, Integrated Performance and resides in the MSFC EV44 Natural Environments Branch.

2.0 DOCUMENTS

2.1 APPLICABLE DOCUMENTS

The following documents include specifications, models, standards, guidelines, handbooks, and other special publications. The documents listed in this paragraph are applicable to the extent specified herein.

TABLE 2.1-1 APPLICABLE DOCUMENTS

Document Number	Document Title
SLS-SPEC-159	Cross-Program Design Specification for Natural Environments

2.2 REFERENCE DOCUMENTS

The following documents contain supplemental information to guide the user in the application of this document.

None.

3.0 MISCELLANEOUS LUNAR AND CIS-LUNAR ENVIRONMENTS

3.1 LUNAR MAGNETIC FIELDS INCLUDING MAGNETIC ANOMALIES

The global magnetic field of the Moon is very weak compared to that of Earth (25000 to 65000 nT or 0.25 to 0.65 gauss for Earth). Measured lunar field strengths were 38, 103, 3, and 327 nT at the Apollo 12, 14, 15, and 16 sites, respectively (Dyal et al. 1974). The Moon does not currently have an internal dynamo to sustain a global magnetic field. Instead, there are regions of anomalously high magnetic fields, commonly referred to as *magnetic anomalies,* generated by crustal magnetic material. In addition, surface features comprised of light and dark albedo regolith called *swirls* are co-located among the largest magnitude crustal anomalies. The magnetic field measured over the Reiner Gamma swirl is approximately 30 nT at 20 km altitude (e.g., Hood 1980, Ravat, et al. 2020, Hood et al. 2021). According to modeling, the strengths of these anomalous fields may reach 500 to 3000 nT at the lunar surface (Hood and Williams 1989, Hemingway and Tikoo 2018), still an order of magnitude below that of Earth. It is unlikely that these fields are of concern for hardware designers.

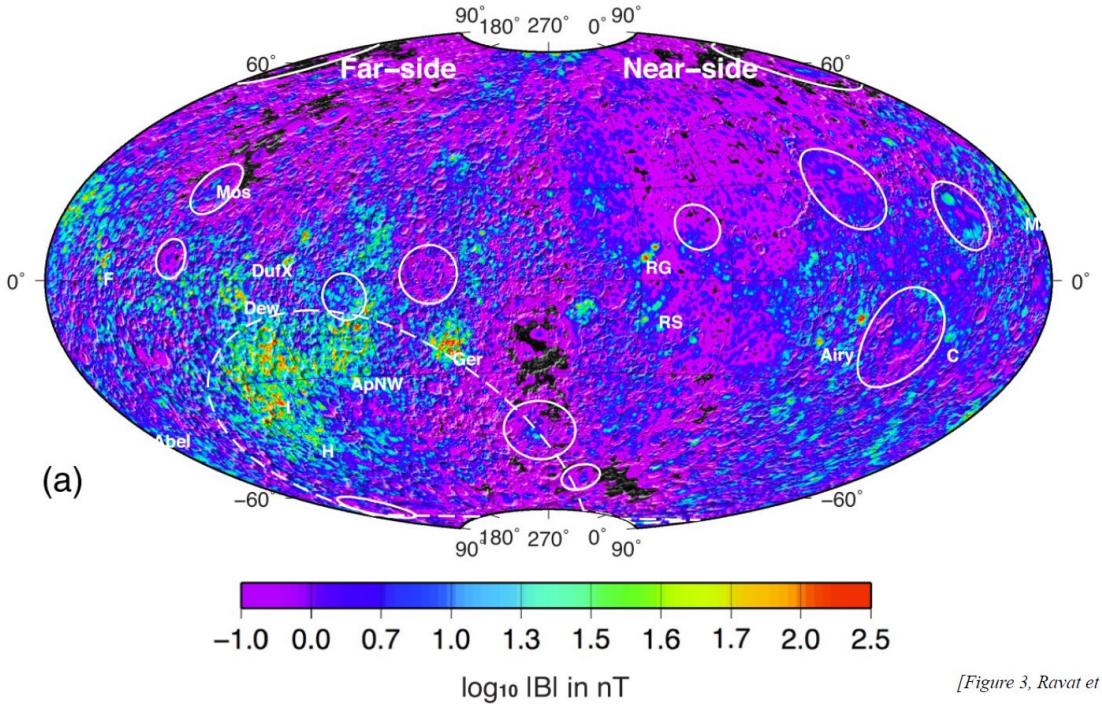

[Figure 3, Ravat et al, 2020]

FIGURE 3.1-1 MAGNETIC FIELD MAP SHOWING MAGNETIC ANOMALIES (RAVAT ET AL. 2020)

Lunar swirls are patches of light and dark regolith associated with unusually high magnetic fields. They are thought to be caused by reduced weathering of the regolith due to stand off of the solar wind by the local magnetic field. The optically brightest regolith correlates with the location of peak magnetic field intensity (Blewett et al., 2011). See Table 3.1-2 for a list of magnetic anomalies studied by Blewett et al., 2011. Solar wind ions and electrons interact differently with the horizontal magnetic field resulting in electrostatic gradients and local ambipolar electric fields (Deca et al., 2014). This forms a density halo and mini-magnetosphere (Kurata et al. 2005; Zimmerman et al. 2015) which causes 10% to 15% of the incident solar wind protons to be reflected (Lue et al., 2011; Deca and Divin, 2016), which reduces space weathering effects that darken regolith. Commercial Lunar Payload Services (CLPS) delivery CP-11 will investigate the Reiner Gamma swirl in 2024 with the Lunar Vertex science payload suite.

TABLE 3.1-1 MAGNETIC FIELD STRENGTH COMPARISONS

Location	Magnetic Field nT	Reference
Earth	25,000 – 65,000	"Geomagnetism Frequently Asked Questions". National Geophysical Data Center. Retrieved 7 July 2022.
Apollo 13, 14, 15	38	Dyal et al. 1974
Apollo 16	327	Dyal et al. 1974
Reiner Gamma	30 at 20km altitude 500 – 3,000 at the surface (modeled)	Hood 1980, Hood et al. 2021 Hood and Williams 1989, Hemingway and Tikoo 2018

TABLE 3.1-2 LUNAR MAGNETIC ANOMALIES FROM BLEWETT ET AL., 2011

Location	Approximate Lat., Long.	Setting	Magnetic Anomaly Strength, nT[a]	Swirl Character
Abel	30°S, 90°E	Mare/highland	10 – moderate	None recognized
Airy	18°S, 3.25°E	Highland	13 – moderate	Loop/dark lane
Crozier	15°S, 51°E	Mare/highland	6 – weak	None recognized
Descartes	15°S, 52°E	Highland	24 – strong	Diffuse bright spot
Firsov	10.5°S, 16.5°E	Highland	11 – moderate	Complex
Gerasimovich	21°S, 236.5°E	Highland	28 – strong	Loop/dark lane
Hartwig	10°S, 280°E	Highland/mare	12 – moderate	None recognized
Hopmann	48.5°S, 160°E	Mare/highland	5 – weak	Complex+loop
Ingenii	33.5°S, 160°E	Mare/highland	20 – strong	Complex
Marginis	16°N, 88°E	Mare/highland	6 – weak[b]	Complex
Moscoviense	27°N, 145°E	Mare	4 – weak	Complex
NW of Apollo	25°S, 197.5°E	Highland	12 – moderate	Loop/dark lane
Reiner Gamma	7.5°N, 302.5°E	Mare	22 – strong	Complex
Rima Sirsalis	8.5°S, 304.5°E	Mare/highland	8 – moderate	Loop/dark lane
Stöfler	40°S, 5°E	Highland	10 – moderate	None recognized

[a]Estimated peak total field strength of magnetic anomaly at 30-km altitude: Weak, <7; moderate, 7–15; strong >15.
[b]Poor coverage by Lunar Prospector magnetometer.

Figure 3.1-2 shows how the mini-magnetosphere formed by a lunar magnetic anomaly can deflect incident solar wind protons and cause an electric field to form.

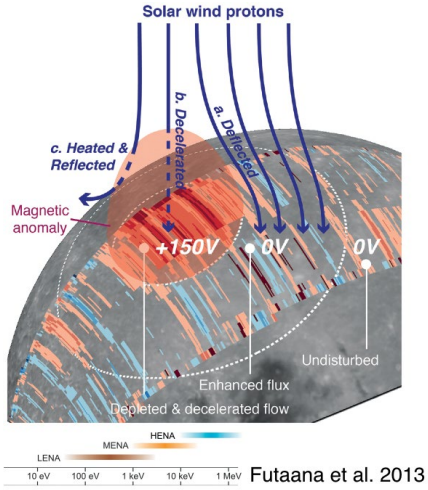

FIGURE 3.1-2. MINI-MAGNETOSPHERES FORM ABOVE LUNAR MAGNETIC ANOMALIES AND CAN DECELERATE IMPINGING SOLAR WIND PROTONS CAUSING AN INCREASE IN SURFACE POTENTIAL, FUTAANA ET AL 2013.

3.2 LUNAR EXOSPHERE DENSITY

The lunar atmosphere, or exosphere, is extremely tenuous with densities ranging from approximately $2x10^5$ particles/cm^3 during the lunar night to 10^4 during the day (Hodges et al., 1975), which is about 14 orders of magnitude less than Earth's atmosphere. The presence of spacecraft hardware generates an exosphere which dominates the natural environment. Vondrak (1974) estimated that each Apollo landing released 10^4 kg of gas on the Moon, roughly equivalent

to the total mass of the lunar exosphere. The Cold Cathode Gauge experiments deployed during Apollo EVAs (Johnson et al., 1970, 1972) were driven off-scale when astronauts came within a few meters and contamination was evident long after the astronauts left.

3.3 LUNAR RADIO NOISE TEMPERATURE

Thermal emissions from the lunar surface are important for link margin analyses for communications systems, but those environments are included in Deep Space Network documentation (JPL 2015, DSN No. 810-005, 105, rev. E, Oct. 2015 or latest version). The information included here is a summary to show how thermal emissions change as a function of lunar phase at various radio frequencies. Brightness temperature as a function of lunar phase was measured by Morabito et al. (2008) at the 34m diameter Deep Space Network Goldstone, California antenna at S-band (2.3 GHz), X-band (8.4 GHz), and Ka-band (32 GHz) frequencies. Figure 10 of that article shows a nearly constant modeled S-band brightness temperature of 228 K, a slightly varying X-band temperature of 235 to 251 K between lunar pre-dawn and late afternoon, and 210 to 278 K at Ka band between pre-dawn and afternoon. Measurements are scattered around those model values.

3.4 REGOLITH ELECTROSTATIC CHARGING/DISCHARGING IN PERMANENTLY SHADOWED REGIONS

The plasma environment and charging at the lunar surface is addressed in DSNE section 3.4.3. Modeling of charging and discharging of the regolith in permanently shadowed regions (PSRs) is discussed in the following: Farrell, W. M. *et al.* (2008) and Zimmerman et al. 2012.

A series of unfortunately named articles in the popular press were published using words like “lightning” and “explosions” to describe an effect thought to be occurring in lunar PSRs (Benson (2016) and Prigg (2017)). There are no lightning strikes occurring in PSRs. These publications stem from a set of articles published that describe the same type of effect occurring in PSRs as happens to spacecraft in any plasma environment. They describe the plasma environment resulting in deep dielectric charging in PSRs and predict dielectric breakdown of the lunar regolith (Jordan et al. 2014). Jordan et al. (2016) states that the energy involved is 0.88 J m-2 yr-1 which is on the order of the flux of meteoroid impact energy and is related to dielectric breakdown of the regolith from exposure to energetic particles.

While some charge may build up in the upper ~1 mm of the PSR regolith, this is not expected to pose any hazard to surface operations. Future measurements may be performed to confirm this.

3.5 EARTHSHINE

The Sun is the primary source of illumination on the lunar surface. However, the sunlit Earth can be a significant source of secondary illumination during the lunar night or in shadowed regions, especially at the lunar poles. Eppler (1991) provides calculations of Earthshine illumination values and comparisons with various lighting conditions on Earth to give a feeling for how useful Earthshine might be. Higher fidelity calculations are given in Glenar et al. 2019. They calculated the broadband Earthshine irradiance to be about 150 mW/m^2 or about ten thousandth that of the

Sun. An observer on the Moon would note that Earthshine is 20-30 times brighter than the Moon at similar phase in the visible part of the spectrum. This is due to the fact that the Earth is larger and its albedo higher than that of the Moon. There are seasonal and monthly variations in the illumination geometry and weather patterns, visible seas, vegetation, and landmasses also affect Earthshine, but it can be a significant source of supplemental illumination when conditions are favorable.

Note that full Earth corresponds to local midnight on the Moon at 0 degrees longitude.

TABLE 3.5-1 COMPARISON OF LIGHTING LEVELS FOR EARTHSHINE, MOON LIGHT AND SUNLIGHT

Units	Full Earth	Full Moon (average distance)	Sunlight
mW/m^2	150	3.4 or 6.8	$1.367x10^6$
Relative to Full Moon	20 - 30	1	
Relative to sunlight	10^{-4}		1

3.6 SOLAR ELEVATION ANGLES DURING APOLLO MISSIONS

Solar elevation angle at the landing site affects landing visibility and thermal analyses. The extremely low solar elevation at the lunar south pole is frequently cited as a challenge to missions there. The solar elevation angles for the Apollo missions are described here for comparison. Apollo missions were timed so that the landings occurred in the local morning hours when low sun angles would improve visibility of surface hazards for landing and EVA mobility. Missions were completed and ascent back to lunar orbit was initiated well before local solar noon when the thermal input from reflected sunlight and emitted infrared radiation from the surface would present the greatest stress to the EMU (Extravehicular Mobility Unit) and vehicle thermal control systems.

This section presents solar elevation angles for each Apollo mission's lunar surface stay along with surface albedo in the vicinity of the lander. These are important parameters for thermal analyses and are provided for comparison with Artemis missions.

Methodology:

The Lunar Reconnaissance Orbiter Camera, a system of three cameras mounted on the Lunar Reconnaissance Orbiter (LRO) that capture high resolution photos of the lunar surface, has a website (LRO Quickmap https://quickmap.lroc.asu.edu) that compiles the photos and locations of interest on a globe. Among these locations of interest are the Apollo missions found by searching in the in-website search bar for "A[*the numbered apollo mission of interest*] LM". By clicking on the landing site indicated by the crosshair, one finds the latitude, longitude, and a host of other

data about that specific location which can be supplemented and augmented with the different overlays, and checkboxes. One such supplement is the albedo data.

To get the rest of the data seen in Figure 3.6-1, the Jet Propulsion Lab Horizons system was used (https://ssd.jpl.nasa.gov/horizons/). At the website, select the celestial body of interest (Sol), either input the latitude and longitude from LROC or input Apollo [mission number of interest]@301, manually check or uncheck the areas and parameters of interest, and input the Apollo ascent and landing dates and times which were obtained with the NASA timeline of events included at the LM Lunar Landing (nasa.gov) site.

Table 3.6-1 compiles the information by mission and provides data on the solar azimuth and elevation at the landing and ascent times. Figure 3.6-2, shows the solar elevation for each mission at the start and end of the mission distinguished by color and with 0 and 180 degrees representing the local horizon.

TABLE 3.6-1 SOLAR ELEVATION, AZIMUTH AND LOCAL ALBEDO FOR APOLLO MISSIONS

	Event	Date	Time UTC	Albedo	Solar Azimuth	Solar Elevation
Apollo 11	Landing	1969-Jul-20	20:17:39	0.078	88.8	10.7
	Ascent	1969-Jul-21	17:54:00		88.9	21.7
Apollo 12	Landing	1969-Nov-19	06:54:36	0.098	91.2	5.1
	Ascent	1969-Nov-20	14:25:47		90.4	21.1
Apollo 14	Landing	1971-Feb-05	09:18:13	0.114	89.6	10.3
	Ascent	1971-Feb-06	18:48:42		88.3	27.3
Apollo 15	Landing	1971-Jul-30	22:16:29	0.094	95.7	12.0
	Ascent	1971-Aug-02	17:11:23		115.3	41.4
Apollo 16	Landing	1972-Apr-21	02:23:35	0.196	86.0	14.8
	Ascent	1972-Apr-24	01:25:47		76.6	50.0
Apollo 17	Landing	1972-Dec-11	19:54:57	0.094	95.9	13.3
	Ascent	1972-Dec-14	22:54:37		115.1	47.8

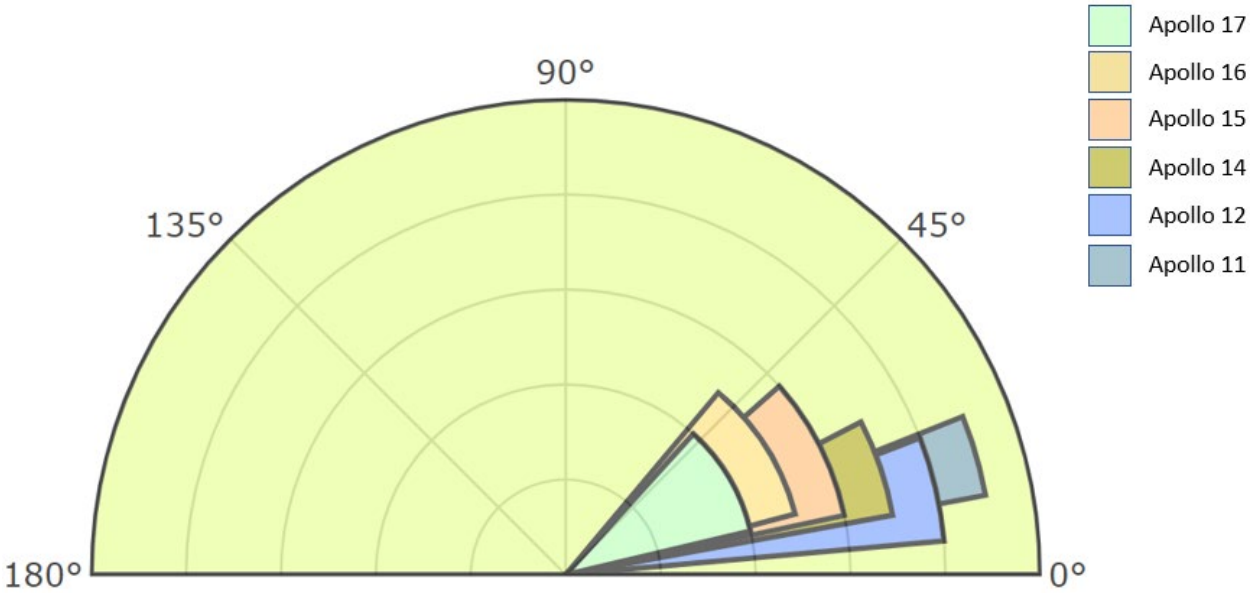

FIGURE 3.6-1 SOLAR ELEVATION ANGLES FOR APOLLO LANDING MISSIONS FROM TIME OF LANDING TO ASCENT TO LUNAR ORBIT

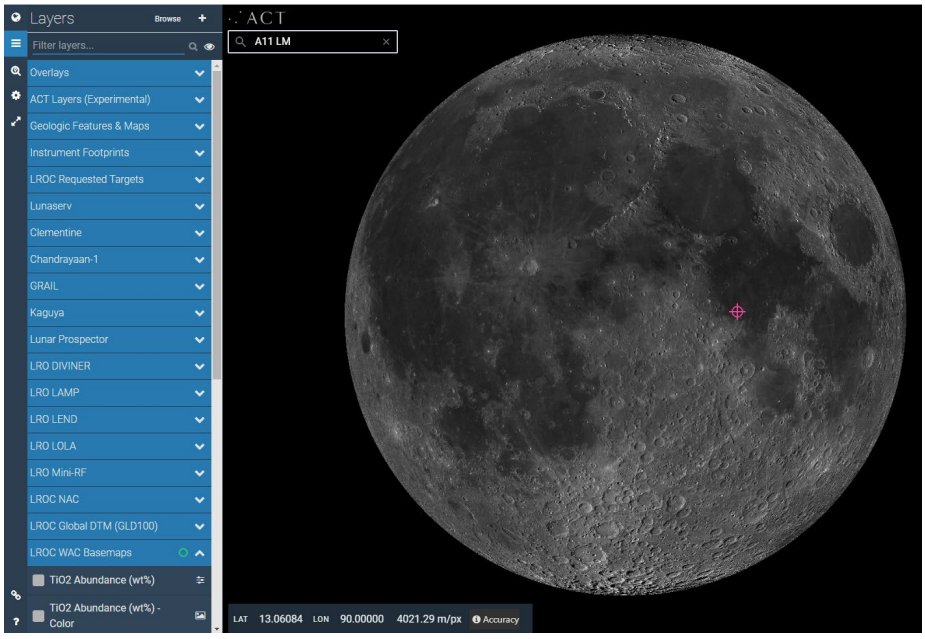

FIGURE 3.6-2 EXAMPLE MISSION LOCATION SEARCH WITH LRO QUICKMAP

3.7 APOLLO MISSION TRAJECTORIES THROUGH THE MAGNETOSPHERE

The work presented here shows important spacecraft charging events from several Apollo, and a representative Artemis mission in a 3D space visualizer. The Apollo missions did not account for

spacecraft charging, but also did not experience adverse effects from the plasma environment due to their trajectories. With respect to the plasma environment, all Apollo missions visited the same region of space: the geomagnetically unshielded region of space between the Earth and Moon but outside of the Earth's magnetotail. Artemis flies with a different concept of operations, placing it in regions of space where these effects cannot be neglected.

Apollo missions avoided the regimes of space that would be considered "high concern" areas of spacecraft charging because of the mission design requiring low temperatures at the landing sites which were mostly at eastern lunar longitudes at fairly low latitudes. Apollo considered the most likely source of vehicle charging to be from friction with the atmosphere and first stage burning (Vance 1964 Effects of Vehicle Electrification on Apollo Electro-Explosive Devices). By 1967 NASA recognized that spacecraft in the solar plasma environment would cause spacecraft charging and that there was a potential to reach high vehicle electric potentials. They modeled 2 environments, a "streaming solar wind" and a "thermalized solar wind" (Shea 1967 Electric Charge on Apollo Command and Service Module in Lunar Environment).

The interaction of the Earth's magnetosphere with the solar wind stretches the Earth's magnetic field in the anti-sunward direction. This is called the magnetotail. Within the magnetotail there is a structure called the plasma sheet (Figure 3.7-1), it is an area of hot plasma in the space between the northern and southern lobes of the magnetotail. This plasma sheet is dynamic and can flap, twist, expand, contract, and warp much like a windsock (Petrukovich 2011). The plasma sheet represents the most severe charging environment in cis-lunar space (DSNE Section 3.3.3.5). The worst-case environment for a discharge to occur during docking would be when the spacecraft are at geosynchronous (GEO) altitudes.

The process to plot important spacecraft charging events in space for any given mission begins by getting the date range for the mission. JPL Horizons was used to get a Sun position for the mission time mid-point. The Sun is considered static for this analysis. Hourly Moon Positions, Earth positions, magnetotail position, and important mission event positions were also computed. The series of points is rotated to set the Sun on the -X axis and the direction of magnetotail in the +X direction. For each of the missions, positions of celestial bodies are verified using 4D-Orbit Viewer, and Apollo trajectory charts where available. All Apollo missions (sans 13) were plotted, as well as a representative Artemis mission.

Figures 3.7-2 through 3.7-7 below are 3-dimensional plots showing Apollo mission trajectories relative to the magnetotail (blue gridline) and plasma sheet (yellow gridline) in. Note that relevant spacecraft events like docking and EVAs happened outside the magnetotail in the solar wind. Excepting Apollo 14, all Apollo missions with a Lunar Module performed a transposition and dock maneuver to extract the landing module before reaching GEO altitudes. Apollo 14 had technical issues with the maneuver before reaching GEO, but finalized docking at 38,000 km altitude. The problems were attributed to foreign debris rather than spacecraft charging (Langley 1972).

A representative Artemis mission trajectory is shown in Figure 3.7-8 for comparison. Note that the Orion spacecraft arrival to the Near Rectilinear Halo Orbit (NRHO) is around New Moon, corresponding to the 12 o'clock position on the figure. A few days later Orion docks with HLS, undocks with HLS, and HLS departs NRHO all before the 10 o'clock position. For the next few days HLS lands on the moon, astronauts conduct EVAs, and HLS launches off the lunar surface just prior to the 6 o'clock position, when the vehicle may be in the plasma sheet. HLS docks and undocks with Orion, and Orion will depart NRHO before the 4 o'clock position on the plot, meaning

these events could occur in the plasma sheet. Each of these events must be analyzed for spacecraft charging concerns, and it may not be possible to move them outside the magnetotail due to other mission constraints.

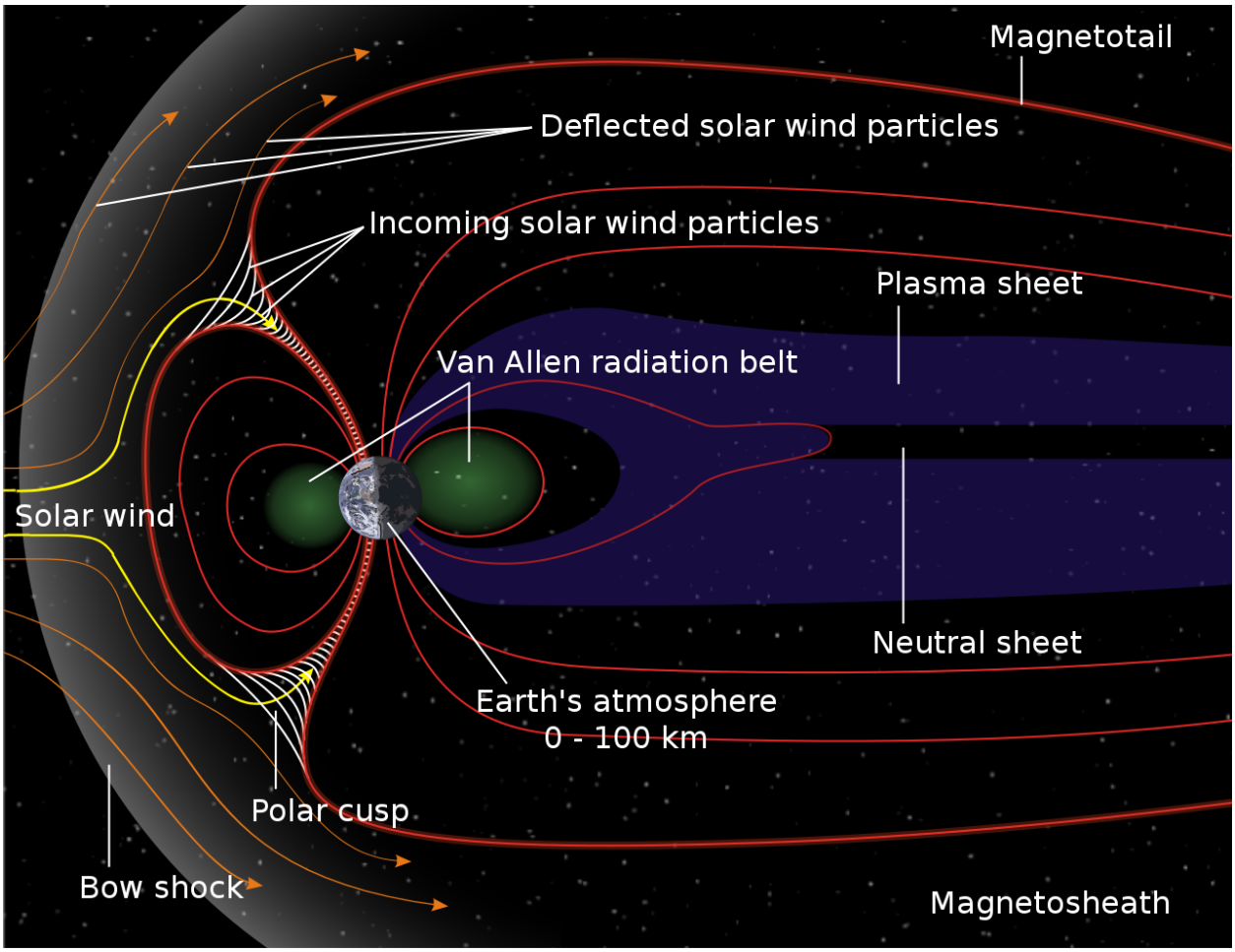

FIGURE 3.7-1 EARTH'S MAGNETOSPHERE (PUBLIC DOMAIN NASA 2014)

APOLLO 11
1969 JULY 16 – 24

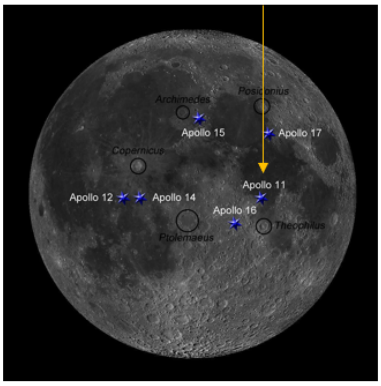

- Regions and locations are approximate
- Magnetopause is dynamic and changes

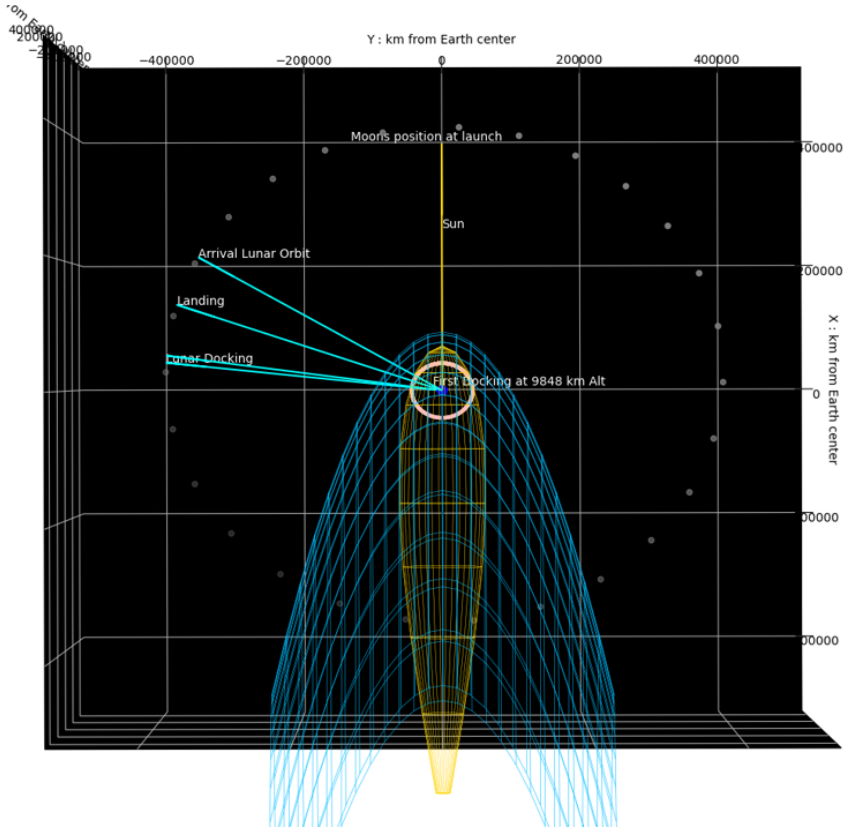

FIGURE 3.7-2 APOLLO 11 MISSION MILESTONES IN THE MAGNETOSPHERE

APOLLO 12
1969 NOV 14 – 24

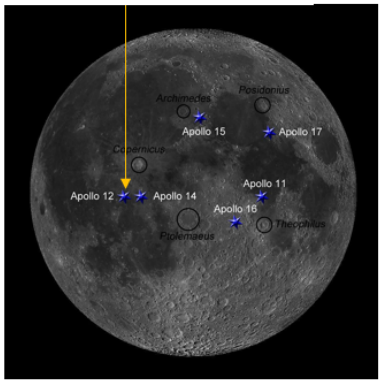

- Regions and locations are approximate
- Magnetopause is dynamic and changes

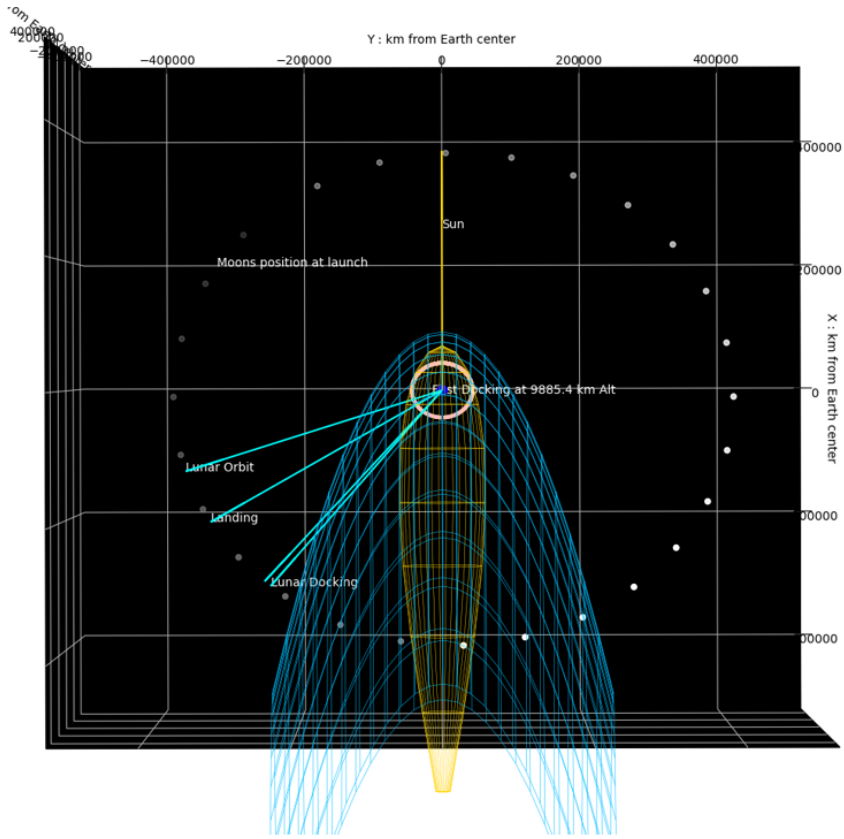

FIGURE 3.7-3 APOLLO 12 MISSION MILESTONES IN THE MAGNETOSPHERE

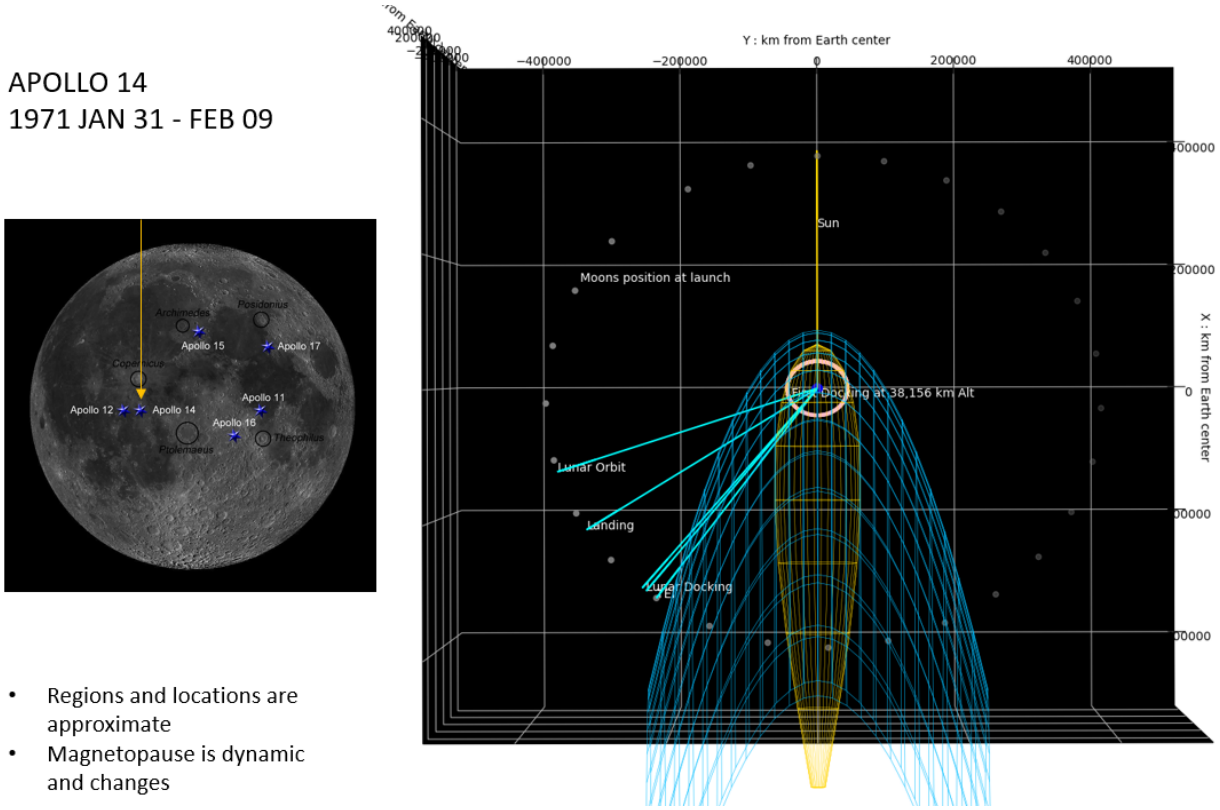

FIGURE 3.7-4 APOLLO 14 MISSION MILESTONES IN THE MAGNETOSPHERE

APOLLO 15
1971 JULY 26 - AUG 07

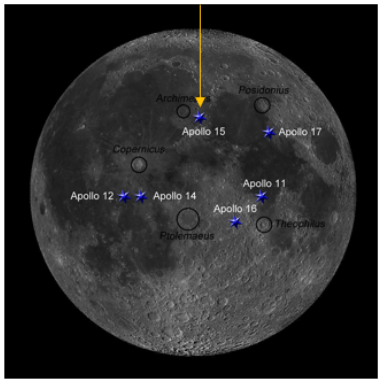

- Regions and locations are approximate
- Magnetopause is dynamic and changes
- TE EVA location is approximate

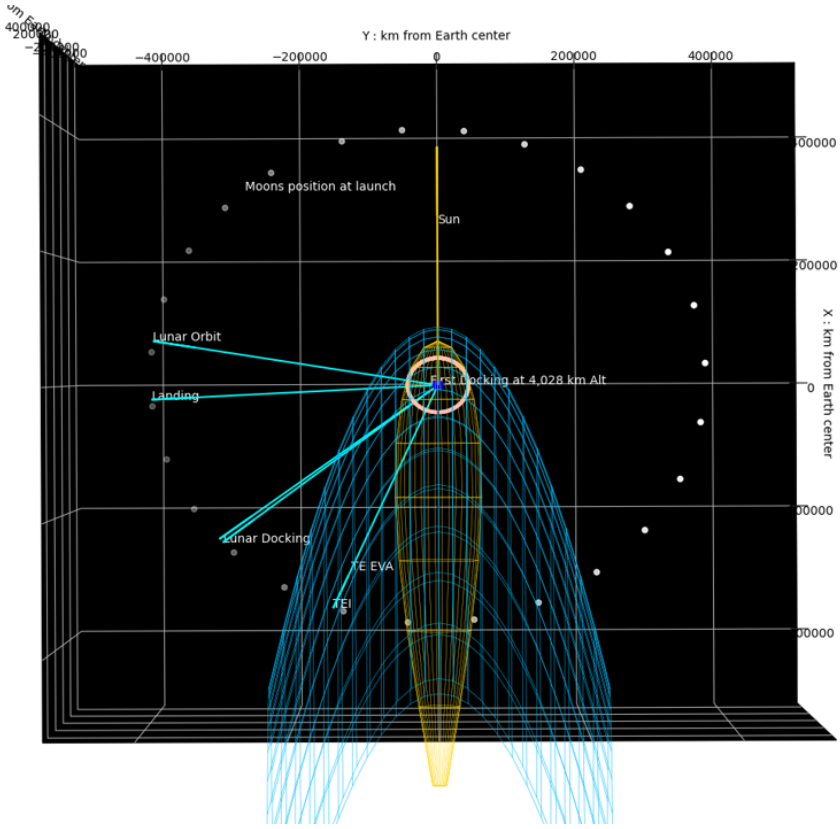

FIGURE 3.7-5 APOLLO 15 MISSION MILESTONES IN THE MAGNETOSPHERE

APOLLO 16
1972 APR 16 – 27

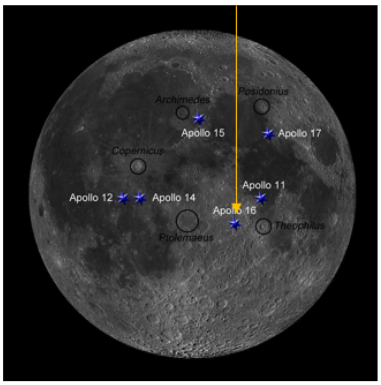

- Regions and locations are approximate
- Magnetopause is dynamic and changes
- TE EVA location is approximate

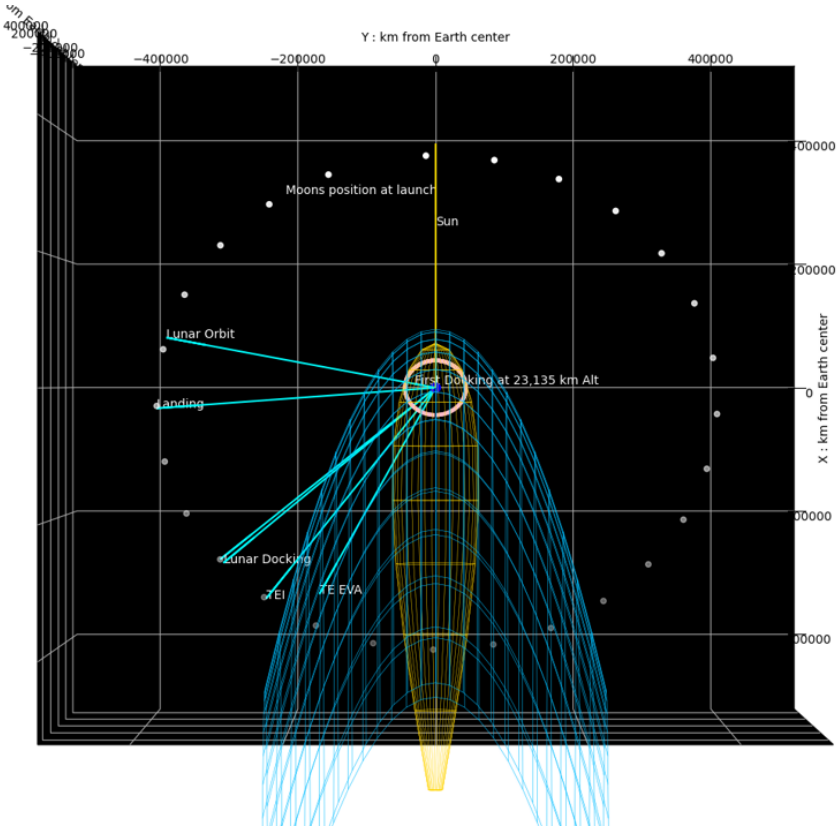

FIGURE 3.7-6 APOLLO 16 MISSION MILESTONES IN THE MAGNETOSPHERE

APOLLO 17
1972 DEC 07 – 19

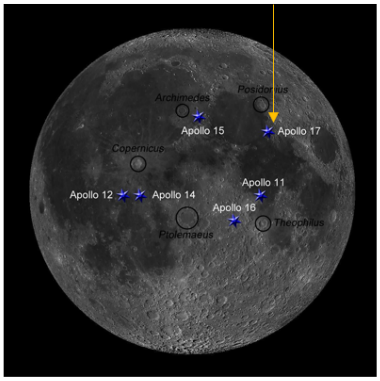

- Regions and locations are approximate
- Magnetopause is dynamic and changes
- TE EVA location is approximate

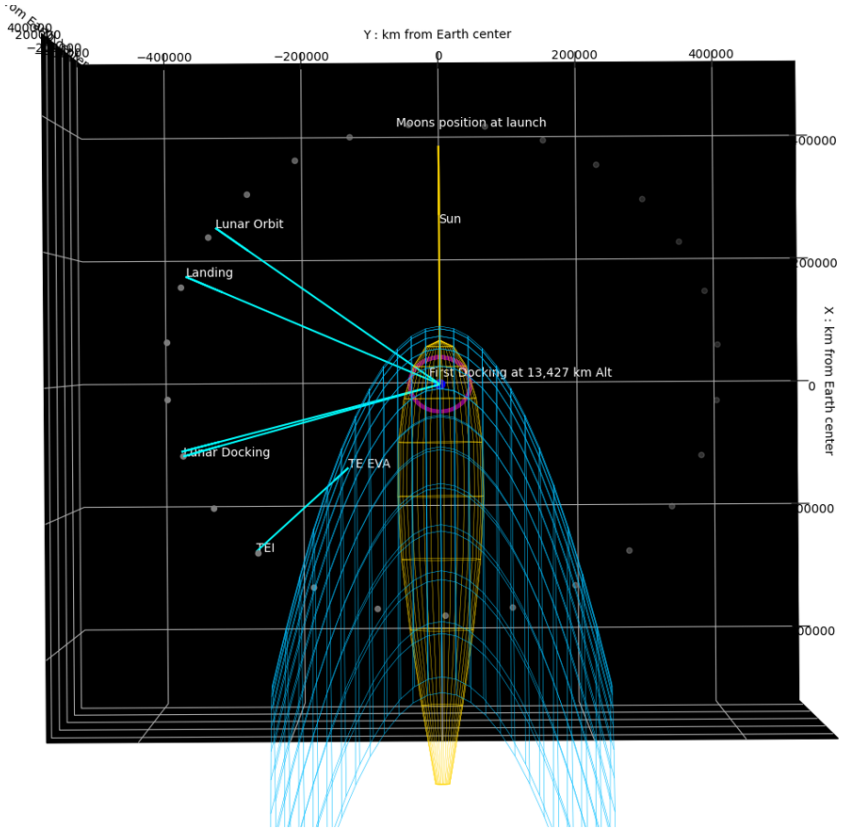

FIGURE 3.7-7 APOLLO 17 MISSION MILESTONES IN THE MAGNETOSPHERE

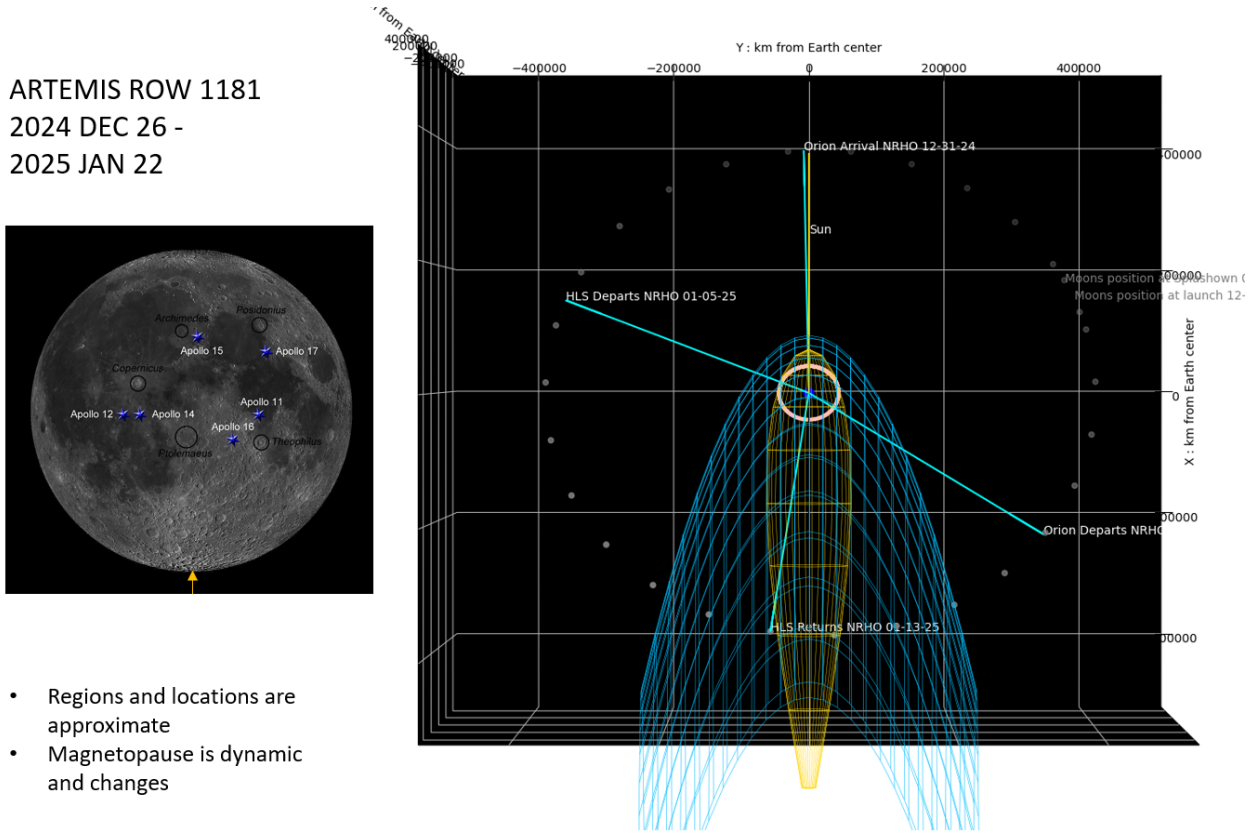

FIGURE 3.7-8 SAMPLE ARTEMIS MISSION LOCATIONS IN THE MAGNETOSPHERE

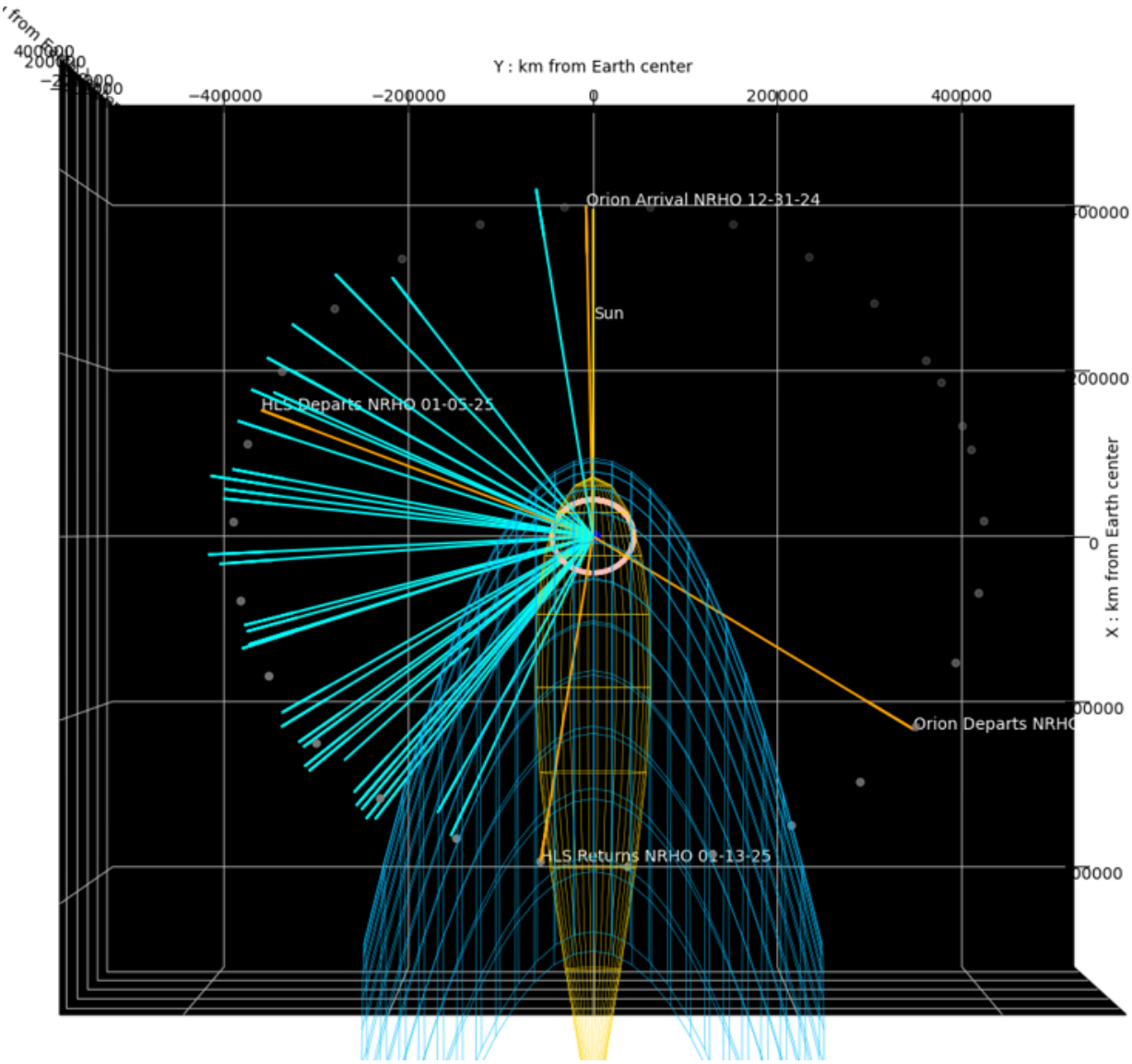

FIGURE 3.7-9 OVERLAY OF ARTEMIS AND APOLLO MISSION LOCATIONS IN THE MAGNETOSPHERE, APOLLO = CYAN, ARTEMIS = ORANGE

3.8 LUNAR PITS AND CAVES

Future lunar exploration missions may explore and exploit lunar caves detected by lunar orbiting imagers. The caves, possibly collapsed portions of lava tubes, could provide a more thermally stable environment due to protection from the extremes of solar heating and deep space radiative environments. Horvath et al. (2022) have developed models of the illumination and thermal environments from LRO measurements. The mass of the roof of the cave will also reduce the flux of ionizing radiation from solar events and galactic cosmic rays and the risk of hypervelocity

impacts from meteoroids and meteoroid impact ejecta. As there are no direct measurements of these environments, no design criteria are currently available. Descriptions of several such features are provided in Wagner and Robinson (2022) and an effort to determine their habitability is described by Lopez-Martinez and Parro (2022).

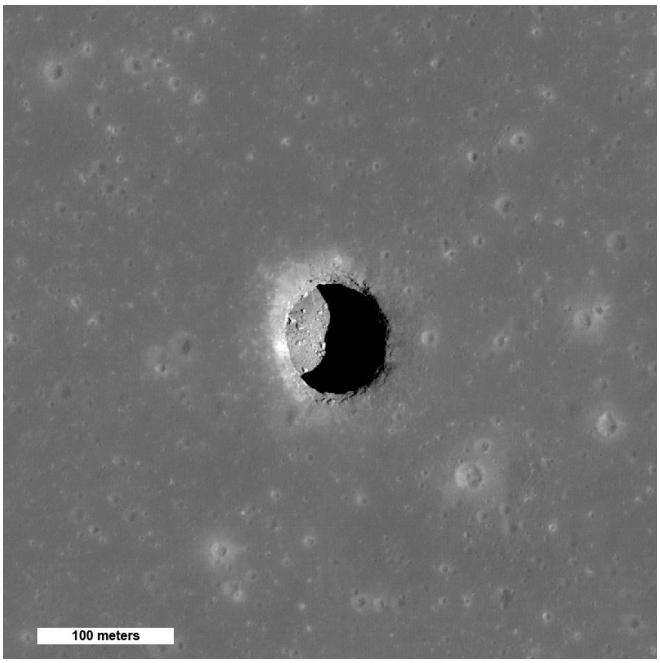

FIGURE 3.8-1 LUNAR PIT IN MARE TRANQUILITATIS FROM LRO NARROW ANGLE CAMERA (IMAGE M126710873R). CREDITS: NASA/GSFC/ARIZONA STATE UNIVERSITY

4.0 REFERENCES

TABLE 4.0-1 REFERENCES

Citation	Complete reference
Apollo 15 Timeline	https://history.nasa.gov/SP-4029/Apollo_15i_Timeline.htm
Benson 2016	Benson, E. Tiny lightning bolt explosions can vaporize the moon’s thin soil, New Scientist Magazine issue 3091, Sept. 2016.
Blewett et al, 2011	Blewett, D., Coman, E., Hawke, B., Gillis-Davis, J., Purucker, M., Hughes, C., 2011. Lunar swirls: examining crustal magnetic anomalies and space weather trends, JGR, Vol 116, Iss E2, CiteID E02002.

TABLE 4.0-1 REFERENCES

Citation	Complete reference
Deca and Divin, 2016	Deca, J., Divin, A., 2016. Reflected charged particle populations around dipolar lunar magnetic anomalies, Astrophysical Journal, Vol. 829, Iss. 2, article id. 60
Deca et al., 2014	Deca, J., Divin, A., Lapenta, G., Lembege, B., Markidis, S., Horanyi, M., 2014. Electromagnetic particle-in-cell simulations of the solar wind interaction with lunar magnetic anomalies, Physical Review Letters, Vol. 112, Iss. 15, id. 151102.
DSN No. 810-005	DSN No. 810-005, 105, rev. E, Oct. 2015
Dyal et al., 1974	Dyal, P., Parkin, C., Daily, W., 1974, Lunar electrical conductivity, permeability, and temperature measurements from Apollo magnetometer experiments, Moon, Vol. 11, p. 406.
Eppler 1991	Eppler, Dean B.,1991. Lighting Constraints on Lunar Surface Operations, NASA-TM-4271
Farrell et al. 2008	Farrell, W. M. et al. ,2008. Concerning the dissipation of electrically charged objects in the shadowed lunar polar regions. Geophys. Res. Lett. 35, 1–5
Futaana et al. 2013	Futaana, Y., Barabash, S., Wieser, M., Lue, C., Wurz, P., Vorburger, A., Bhardwaj, A., and Asamura, K. (2013), Remote energetic neutral atom imaging of electric potential over a lunar magnetic anomaly, Geophys. Res. Lett., 40, 262– 266, doi:10.1002/grl.50135.
Glenar et al. 2019	Glenar, David A., Stubbs, Timothy J., Schwieterman, Edward W., Robinson, Tyler D., Livengood, Timothy A., 2019. Earthshine as an illumination source at the Moon, Icarus, 321, 841-856.
Halekas et al., 2009	Halekas, J. S., Delory, G. T., Lin, R. P., Stubbs, T. J. & Farrell, W. M., 2009. Lunar surface charging during solar energetic particle events: Measurement and prediction. J. Geophys. Res. Sp. Phys. 114, 1–16
Hemingway and Tikoo 2018	Hemingway, D. and Tikoo, S., 2018. Lunar swirl morphology constrains the geometry, magnetization, and origins of lunar magnetic anomalies, JGR: Planets, Vol. 123, Iss. 8, p. 2223-2241.
Hodges et al., 1975	Hodges, R. Jr., 1975. Formation of the Lunar Atmosphere, The Moon, Vol. 14, Issue 1, pp. 139-157.
Hood 1980	Hood, L., 1980. Bulk magnetization properties of the Fra Mauro and Reiner Gamma formations, Lunar and Planetary Science Conference, 11th, Vol. 3 (A82-22351 09-91), p. 1879-1896.

TABLE 4.0-1 REFERENCES

Citation	Complete reference
Hood and Williams 1989	Hood, L., Williams, C., 1989. Lunar and Planetary Science Conference, 19th, Proceedings (A89-36486 15-91), p. 99-113.
Hood et al. 2021	Hood, L., Torres, C., Oliveira, J., Wieczorek, M., Stewart, S., 2021. A new large scale map of the lunar crustal magnetic field and its interpretation, JGR: Planets, Vol. 126, Iss. 2, article id. e06667.
Horvath et al. 2022	Horvath, T., Hayne, P., Paige, D., 2022. Thermal and illumination environments of lunar pits and caves: models and observations from the Diviner Lunar Radiometer Experiment, Geophysical Research Letters, Vol. 49, Iss 14, article id. e99710
Johnson et al., 1970	Johnson, F., Evans, D., Carroll, J., 1970. Apollo 12: Preliminary Science Report. NASA SP-235, p. 93.
Johnson et al., 1972	Johnson, F., Carroll, J., Evans, D., 1972. Vacuum measurements on the lunar surface, J. Vac. Sci. Technol., Vol. 9, p. 450 - 456.
Jordan, et al. 2014	Jordan A., Stubbs, T., Wilson, J., Schwadron, N., Spence, H., Joyce, C., 2014. Deep dielectric charging of regolith within the Moon's permanently shadowed regions. Journal of Geophysical Research: Planets, 119, 1806-1821.
Jordan et al.2016	Jordan, A., Stubbs, T., Wilson, J., Schwadron, N, Spence, H., 2016. The rate of dielectric breakdown weathering of lunar regolith in permanently shadowed regions. Icarus, vol. 283, pp. 352-358.
JPL DSN	DSN No. 810-005, 105, rev. E, Oct 2015
JPL Horizons	JPL Horizons (ssd.jpl.nasa.gov/horizons/)
Kurata et al., 2005	Kurata, M., Tsunakawa, H., Saito, Y., Shibuya, H., Matsushima, M., Shimizu, H., 2005. Mini-magnetosphere over the Reiner Gamma magnetic anomaly region on the Moon, Geophysical Research Letters, Vol. 32, Iss. 24, CiteID L24205.
Langley 1972	https://ntrs.nasa.gov/citations/19730010157
LM Lunar Landing	https://history.nasa.gov/SP-4029/Apollo_18-27_LM_Lunar_Landing.htm
Lopez-Martinez and Parro 2022	Lopez-Martinez, G., Parro, L., 2022. Are pit craters habitable? Geological analysis and description of their structural potential as lunar bases, 16th Europlanet Science Congress, id. EPSC2022-604.
LROC QuickMap	https://quickmap.lroc.asu.edu
Lue et al., 2011	Lue, C., Futaana, Y., Barabash, S., Wieser, M., Holmstrom, M., Bhardwaj, A., Dhanya, M., Wurz, P., 2011. Strong

TABLE 4.0-1 REFERENCES

Citation	Complete reference
	influence of lunar crustal fields on the solar wind flow, Geophysical Research Letters, Vol., 38, Iss. 3, CiteID L03202
Lunar Sourcebook	Heiken, G., Vaniman, D., French, B., editors, 1991. Lunar Sourcebook: A User's Guide to the Moon, https://www.lpi.usra.edu/publications/books/lunar_sourcebook/
Morabito et al., 2007	Morabito, David & Imbriale, W.A. & Keihm, Stephen, 2007. Observing the Moon at Microwave Frequencies Using a Large-Diameter Deep Space Network Antenna, IEEE Transactions on Antennas and Propagation. 56. 650 - 660. 10.1109/TAP.2007.915471
National Geophysical Data Center	"Geomagnetism Frequently Asked Questions"
Petrukovich 2011	Petrukovich, A. A., 2011. Origins of plasma sheet By, J. Geophys. Res., 116, A07217
Prigg 2017	Prigg, M., The incredible sparking soil on the Moon: NASA reveals solar storms can cause ‘miniature lightning strikes’. Dailymail.com, 6 Jan. 2017.
Ravat et al., 2020	Ravat, D., Purucker, M., Olsen, N., 2020. Lunar magnetic field models from lunar prospector and SELENE/Kaguya along-track magnetic field gradients, JGR: Planets Vol., 125, Iss. 7, article id e06187
SLS-SPEC-159 DSNE	Cross-Program Design Specification for Natural Environments https://ntrs.nasa.gov/citations/20210024522
Stubbs et al., 2007	Stubbs, T. J., Halekas, J. S., Farrell, W. M. & Vondrak, R. R., 2007. Lunar surface charging- A global perspective using Lunar Prospector data. in Dust in Planetary Systems, ESA SP-643 1–4
Vance et al., 1964	Vance, E., Seely, L., Nanevicz, J., 1964. Effects of Vehicle Electrification on Apollo Electro-Explosive Devices. Final Report, Stanford Research Institute, Contract NAS 9-3154.
Vondrak 1974	Vondrak, R., 1974. Creation of an artificial lunar atmosphere, Nature, Vol 248, Issue 5450, p. 657-659.
Wagner and Robinson 2022	Wagner, R., Robinson, M., 2022. Lunar pit morphology: implications for exploration, JGR: Planets, Vol. 127, Iss. 8, article id. e07328.
Zimmerman et al. 2015	Zimmerman, M., Farrell, W., Poppe, A., 2015. Kinetic simulations of kilometer-scale minimagnetosphere formation on the Moon, JGR: Planets, Vol. 120, Iss. 11, p. 1893-1903.
Zimmerman et al., 2012	Zimmerman, M. I., Jackson, T. L., Farrell, W. M. & Stubbs, T. J., 2012. Plasma wake simulations and object charging in a

TABLE 4.0-1 REFERENCES

Citation	Complete reference
	shadowed lunar crater during a solar storm. J. Geophys. Res. E Planets 117, 1–11

APPENDIX A
ACRONYMS AND ABBREVIATIONS

A1.0 ACRONYMS AND ABBREVIATIONS

TABLE A1-1 ACRONYMS AND ABBREVIATIONS

CLPS	Commercial Lunar Payload Services
cm	centimeter
DSNE	Cross-Program Design Specification for Natural Environments, SLS-SPEC-159
DSNE	Deep Space Network
EMU	Extravehicular Mobility Unit
EVA	extravehicular activity
GEO	geosynchronous orbit
GHz	gigahertz
GSFC	Goddard Space Flight Center
HLS	Human Landing System
IEEE	Institute of Electrical and Electronics Engineers
JPL	Jet Propulsion Laboratory
kg	kilogram
km	kilometer
LRO	Lunar Reconnaissance Orbiter
LROC	Lunar Reconnaissance Orbiter Camera
m	meter
MSFC	Marshall Space Flight Center
mW	milliwatt
NRHO	near rectilinear halo orbit
nT	nanoTesla
OPR	Office of Primary Responsibility